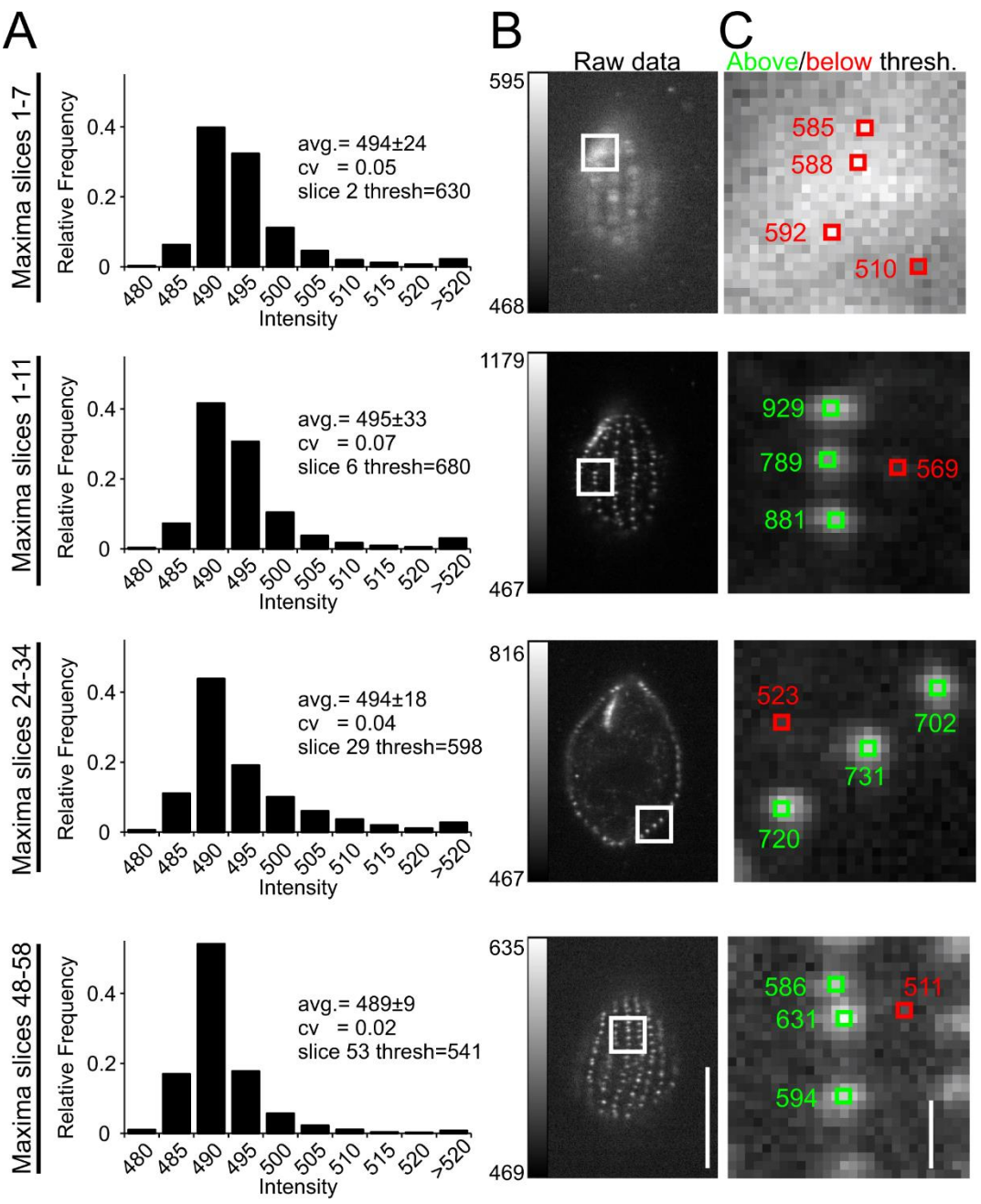

Fig. S1. An adaptive thresholding approach to identify BBs in thick image stacks. (A) Relative frequency distributions of all the local maxima within the indicated image planes of a representative *Tetrahymena* confocal image stack. The analysis routine assesses the intensity profile of maxima within a rolling Z-range and assigns a threshold based on the coefficient of variation. Since the coefficient of variation will be higher for slices that have a mix of high intensity objects and low intensity background, the routine assigns a higher threshold for slices with a greater coefficient of variation. (B) Sample planes from the raw data corresponding to the frequency distributions in (A). Bar, 15 μm. (C) Zoomed in insets of the boxes outlined in (B) showing the intensity of BB maxima (green) and background maxima (red) to highlight the accuracy of the adaptive threshold. Bar, 1 μm.

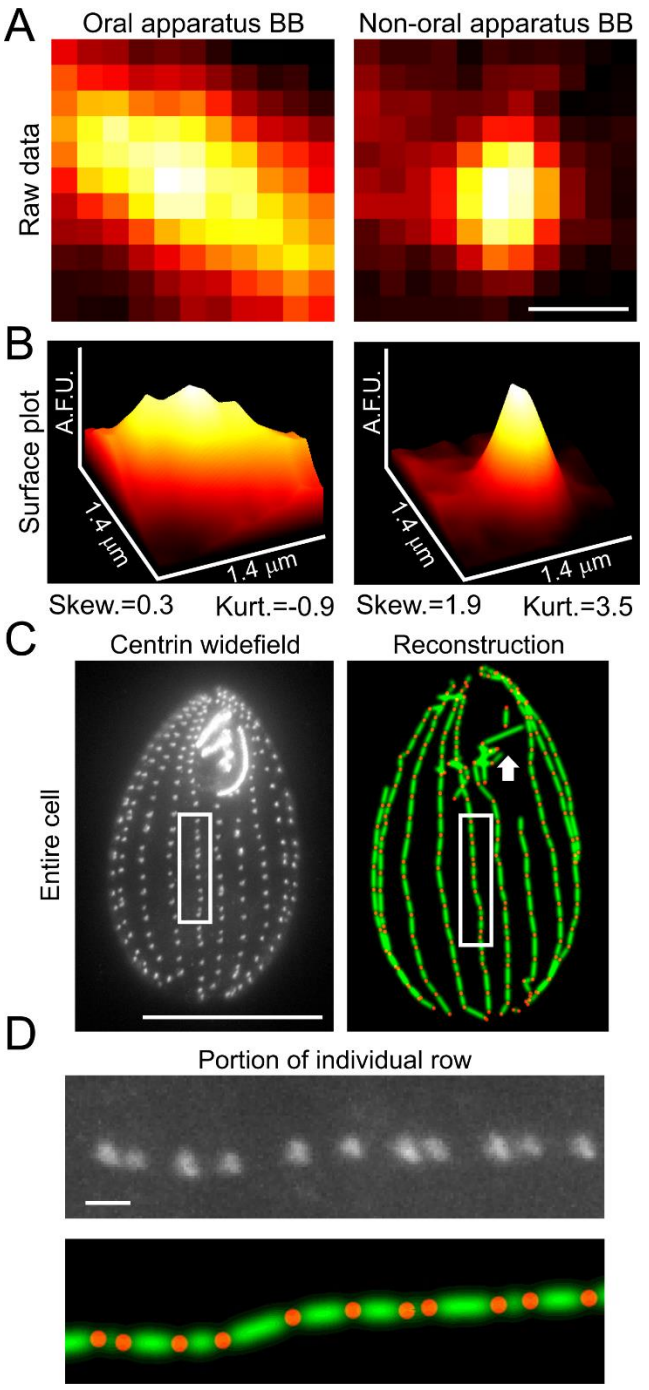

Fig. S2. Oral apparatus BBs have a unique intensity profile when compared to cortical BBs and the analysis of widefield images. (A) Images showing a representative oral apparatus BB (left) and a cortical BB (right) displayed using a heat map LUT. Bar, 0.5 µm. (B) Surface plots of the same images showing the homogenous intensity profile of the oral apparatus BB (left) and the sharply peaked intensity profile of the cortical BB (right). The values beneath each surface plot are the descriptors of the intensity histogram for each image showing that the skewness and kurtosis can be used to separate the two classes of BB. (C) A *Tetrahymena* cell stained with centrin and imaged using a widefield fluorescence microscope (left) and the corresponding reconstruction (right) demonstrating that the image analysis routine is sensitive enough to produce reconstructions of both widefield and confocal images. The increased intensity of the oral apparatus BBs increases the incidence of BB misidentifications in the widefield images (white arrows). Bar, 15 µm. (D) Enlarged regions of the white box in (D) show the accuracy in reconstructing individual ciliary rows within the medial quadrants. Bar, 1 µm.

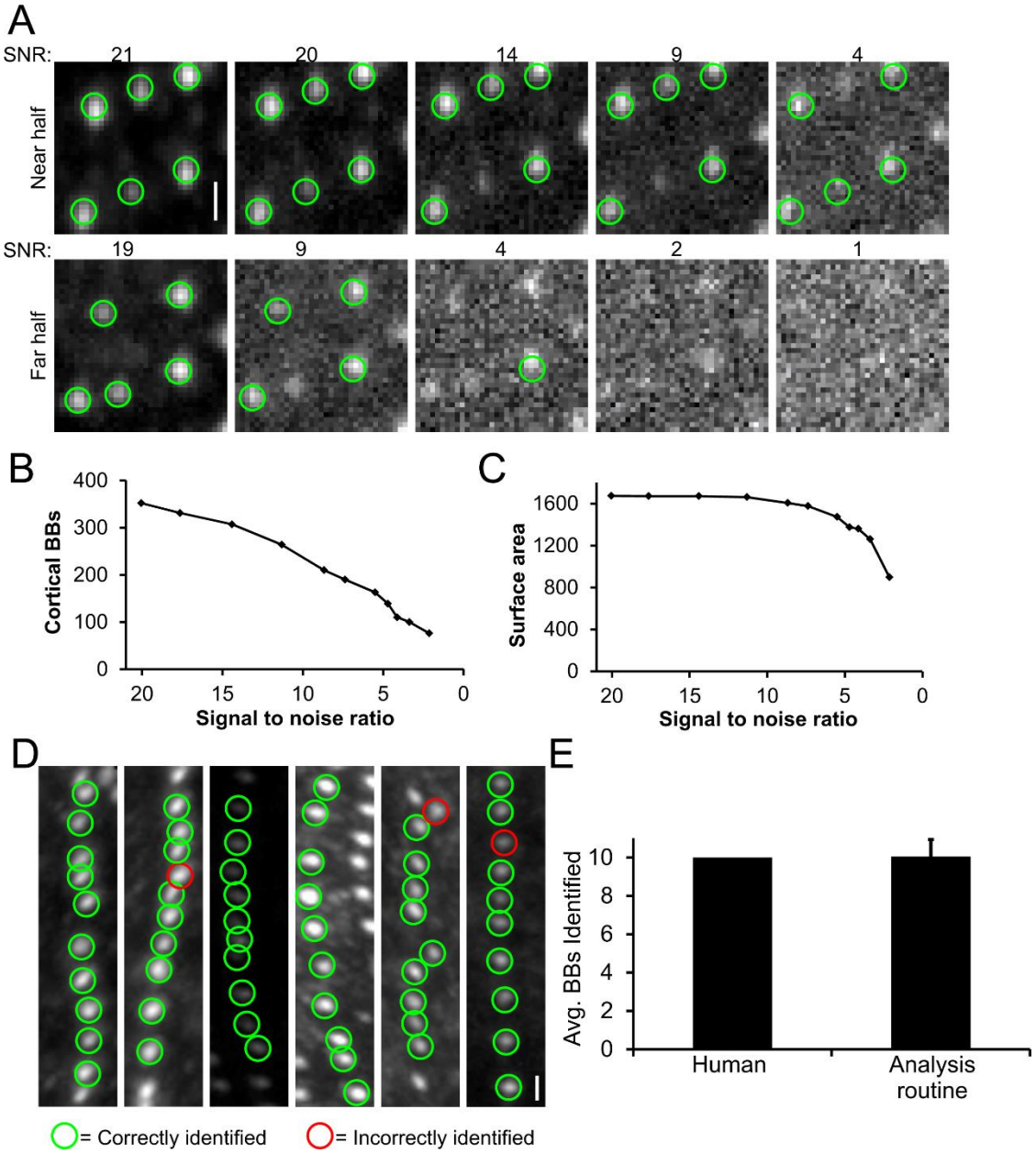

Fig. S3. Evaluating the robustness of the image analysis routine and comparing the image analysis routine against a human observer. (A) Gaussian noise was added to a *Tetrahymena* image and the resulting signal-to-noise ratio (SNR) was calculated for regions in the front (bright) and back (dim) halves of the cell. Green circles represent analysis routine identified BBs in each image. Bar, 1 μm. As the SNR decreases (left to right), the image analysis routine's ability to detect BBs decreases (B). This negatively impacts the ability of the analysis routine to calculate a reliable surface area (C) because the dim BBs on the back half of the cell are preferentially lost, which distorts the 3D convex hull-generated measurements. (D) A human observer scored 10 consecutive BBs on 20 different cells blind to the outcome of the automated image analysis routine. Six representative images show the human identified BBs (green circles) along with analysis errors (red circles). The scored BBs were in the medial longitudinal quadrants of the cell. Bar, 1 μm. (E) The image analysis routine detected 201 BBs out of a possible 200 (average of 10.05 per cell). There were six false positives where the image analysis routine misidentified noise as a BB, and there were five false negatives were the analysis routine did not detect a BB for a total of 11 errors. We estimate the overall error rate of the image analysis routine to be approximately 5% in the medial quadrants of the cell.

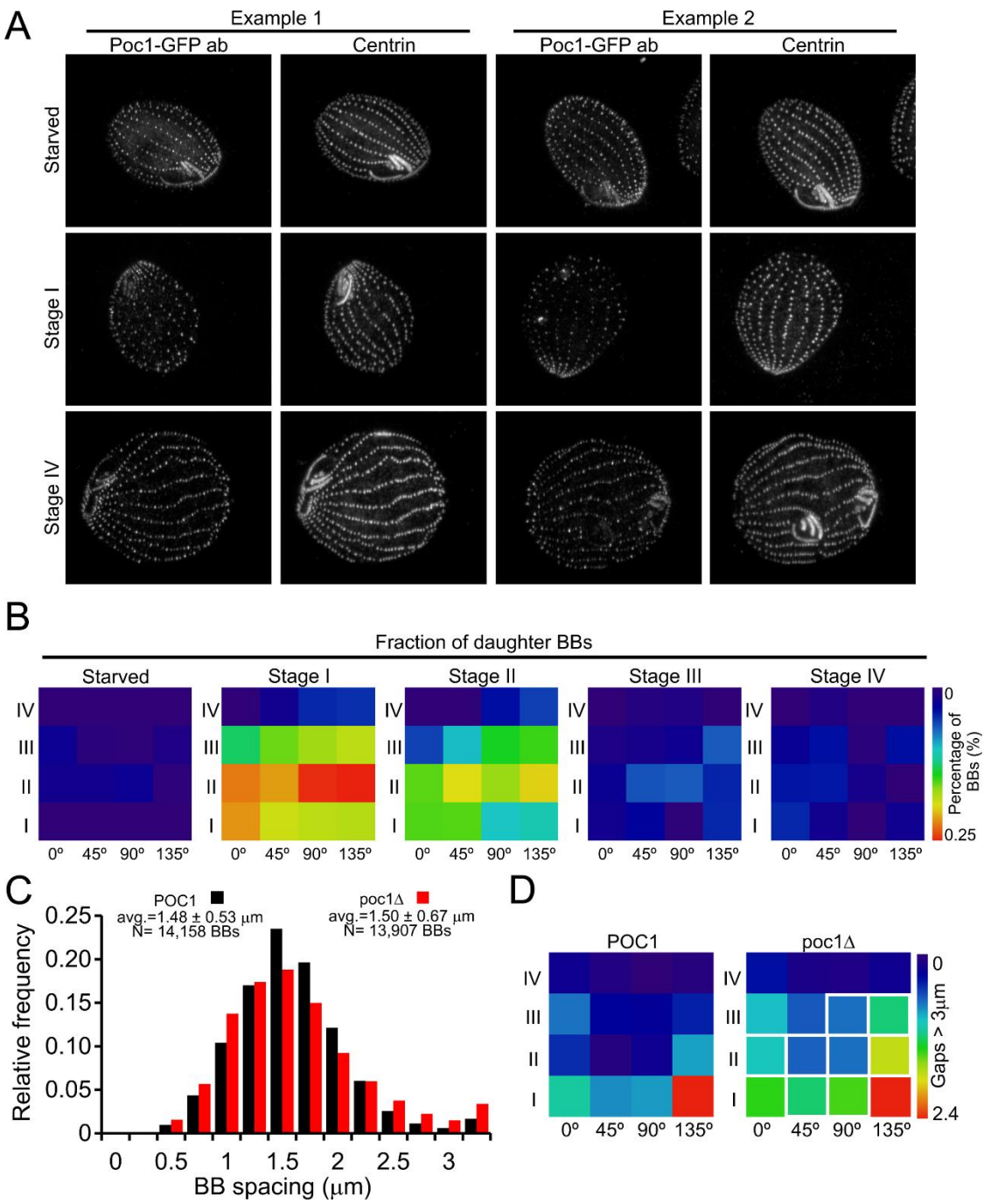

Fig. S4. Identifying the frequency of new BB assembly in spatial domains and quantifying BB spacing in *poc1*Δ cells. (A) Representative images of cells at the indicated stage stained with centrin and a GFP antibody to detect Poc1:GFP. Two representative cells are shown for each condition. (B) Heat maps showing the fraction of total cortical BBs that have an anterior/posterior Poc1 intensity ratio less than 2 fold and are thus considered to be nascent daughter BBs (see Figure 4). The heat maps show that the greatest fraction of daughter BBs are found in the medial and posterior portions of the cell. (C) Relative frequency distribution of BB spacing for POC1 (black) and *poc1*Δ (red) cells. (D) Heat maps showing the average number of BB spacing gaps > 3 µm within the spatial domains of POC1 (left) and *poc1*Δ (right) cells. White boxes denote statistical significance. The histograms (C) and heat maps (D) depict cells combined from the 25°C and 37°C data sets.